Research Article

Rajendran Selvamani*, Loganathan Rubine, Prabhakaran Thangamuni, Rossana Dimitri, Francesco Tornabene

Analysis of magneto-aerothermal load effects on variable nonlocal dynamics of functionally graded nanobeams using Bernstein polynomials

https://doi.org/10.1515/cls-2025-0029
received November 18, 2024; accepted May 11, 2025

Abstract: This study explores the relationship between the variable nonlocal parameter and material variations in functionally graded (FG) nanobeams incorporating the influence of unsteady aero thermal and magnetic load defined by the first-order Piston theory. The governing equations of FG Euler nanobeams are derived using Eringen's nonlocal elasticity theory. These equations are then numerically tested using the Bernstein-based Rayleigh-Ritz method. A comparison with previously published results is conducted to validate the accuracy of the findings. Additionally, the study investigates the effects of nonlocal ceramic, nonlocal metal parameters, Mach number, and aerodynamic force on various physical parameters of FG nanobeam.

Keywords: FG Euler nanobeam, variable nonlocal elasticity, Rayleigh-Ritz technique, Bernstein polynomials, Piston theory

1 Introduction

Functionally Graded nanobeams with customized properties can greatly improve Micro-Electro-Mechanical Systems devices, making them more reliable and efficient. These advancements can also benefit Nano-Electro-Mechanical Systems devices, leading to innovations in sensing, actuation, and signal processing for various applications, including communication systems and quantum computing. Additionally, integrating these nanobeams into implantable sensors or drug delivery systems can offer precise monitoring of health parameters and controlled release of medications. A class of Japanese scientists initiated a development in functionally graded materials (FGMs) as a type of composite to regulate the volume fractions of two or more materials in the mixture. Ebrahimi *et al.* [1,2] presented a study on wave scattering in viscoelastic functionally graded (FG) nano beams. Furthermore, within the context of shear bending in third mode deformation theory, vibration features of Magneto Thermo Electro Elastic FG nanobeams were studied by Ebrahimi and Barati [3]. A new higher-order shear deformation theory (HSDT) for the analysis of buckling and free vibration in isotropic and FG sandwich beams was put forth by Nguyen *et al.* [4]. Alibeigi *et al.* [5,6] introduced the buckling behavior of nanobeams using the Euler-Bernoulli beam model with the inclusion of von Kármán geometrical nonlinearity. Furthermore, Shariati *et al.* [7] investigated the bending of size-dependent magneto-electro-elastic (MEE) nanobeams over nonlinear substrate. Some studies by Ebrahimi *et al.* [8] have been carried out encompassing diverse facets. These include studies on the loading of hygro-thermal and bending of electromagnetically responsive piezoelectric nanobeam systems, progressive analysis of intelligent nanostructures, and frequency assessment of FG thin beams after thermal post-buckling. Additionally, the distinction of elastic nanobeams driven by stress and strain has been addressed through integral elasticity in references Li *et al.* [9] and Romano and Barretta [10].

A study by Barretta *et al.* [11] employed the kinematic model to investigate buckling in beams composed of FG materials subjected to multiple thermal loads. The work of Kiani and Eslami [12] focused on analyzing the propagation of waves in infinite FG plates within a thermal environment. Sun and Luo [13], Thai and Choi [14] developed a consistently refined HSDT to examine the free vibration of FG plates resting on an elastic foundation and to explore the impact of boundary conditions on natural frequencies.

* **Corresponding author: Rajendran Selvamani,** Department of Mathematics, Karunya Institute of Technology and Sciences, Coimbatore, 641114, Tamilnadu, India, e-mail: selvamani@karunya.edu
Loganathan Rubine, Prabhakaran Thangamuni: Department of Mathematics, Karunya Institute of Technology and Sciences, Coimbatore, 641114, Tamilnadu, India
Rossana Dimitri, Francesco Tornabene: Department of Innovation Engineering, University of Salento, Lecce, Italy

Thai *et al.* [15] studied the nonlinear bending in nanobeams was discussed using the (FEM) finite element method. A study by Reddy and El-Borgi [16] surveyed the variation of natural frequencies using the nonlocal theory on a viscoelastic sheet. Analyzing size-dependent elements of beams was an objective of Ebrahimi and Barati [17]. Graphene sheets were used to model thermo-elastic problems *via* nonlocal strain gradient theory by Lim *et al.* [18]. Ebrahimi and Mokhtari [19] analyze the transverse vibrations of rotating porous FG beams using the differential transform method, highlighting the effects of porosity, rotational speed, and material gradation on natural frequencies. Ebrahimi and Salari [20] the buckling response of a nanobeam was investigated by applying the Euler-Bernoulli theory *via* shear models. Another study by Vinh and Tounsi [21] explored the Timoshenko beam theory to examine reliable temperature rise, and external electric and magnetic potential, incorporating nonlocal formulations for MEE vibrations. This analysis considered different thermal loads, as well as the influence of electrical and magnetic fields. Additionally, the bending characteristics of MEE nanobeams were thoroughly investigated by Karmakar and Chakraverty [22]. Additionally, Li and Hu [23] delved into examining the influence of scale-oriented wave propagation in different physical moduli. Ke and Wang [24] presented findings on the vibration of FG sandwich nanoplates. The paper of Mohamed *et al.* [25] explores the nonlinear coupled axial-lateral vibration of functionally graded fiber-reinforced composite laminated (FG-FRCL) cantilever beams under aero-thermal loads. Selvamani *et al.* [26–29] explore the wave propagation behavior of nonhomogeneous porous Euler nanobeams using Bernstein polynomials (BPs) to model boundary characteristics. Alimoradzadeh *et al.* [30] discussed by nonlinear axial-lateral coupled vibration of FG-FRCL beams subjected to aerothermal loads. Tao *et al.* [31] discussed the nonlinear dynamic behaviors of fiber metal laminated beams subjected to moving loads under thermal environments. The objective of this study is to explore the effects of nonlinear thermal vibration on a fluid-infiltrated porous nanobeam, taking into account nonlocal variables. The structure of this paper is outlined as follows: Section 2 presents the fundamental equations governing the behavior of the FG nanobeam under aerothermal loads, while Section 3 discusses the theoretical foundations of the BP method. Section 4 employs the Rayleigh–Ritz-based BP method to solve for the stiffness and mass matrix. Section 5 details the orthogonal Bernstein polynomial (OBP) method. Section 6 presents a convergence theorem to prove the results from the above method. Section 7 provides a comprehensive validation of the proposed model through comparison with existing literature and experimental data. Finally, a summary of the conclusions along with graphical results is presented.

2 Problem formulation

An examination of thermo-electro-magneto FGM has been carried out using the refined higher-order state space strain gradient theory. The nanobeam possesses dimensions including length (L), width (b), and thickness (h). The FGM, in this case, is comprised of two distinct sections: a ceramic segment and a metallic segment. In order to accommodate behaviors influenced by temperature, the study incorporates an analysis of the individual components within the FGM (Figure 1).

In this section, the properties have been computed using power-law relations. To ascertain these properties along the thickness direction concerning temperature, the volume fractions of the metallic and ceramic phases are calculated using the power law model. Consequently, the fractional volume of the ceramic part can be [4],

$$V_c = \left(\frac{z}{h} + \frac{1}{2}\right)^P, \tag{2.1}$$

while the exponential power law and thickness explore the property distributions in each layer of the nanobeam, and the property of material values are considered at local temperature as [2],

$$P = P_0(P_{-1}T^{-1} + 1 + P_1T + P_2T^2 + P_3T^3), \tag{2.2}$$

whereas $P_0, P_{-1}, P_1, P_2, P_3$ are the coefficients of material phases. The volume fraction is taken as $V_m + V_c = 1$.

The material properties of nonlocal FGM, including Young's modulus (E), mass density (ρ), and Poisson's ratio (ν) can be achieved

$$\begin{aligned} E(z) &= E_cV_c + E_mV_m \\ \rho(z) &= \rho_cV_c + \rho_mV_m \\ \nu(z) &= \nu_cV_c + \nu_mV_m. \end{aligned} \tag{2.3}$$

Additionally, the HSDT provides insight into these stress–strain changes. By considering the refined deformable shear beam's direction as [4],

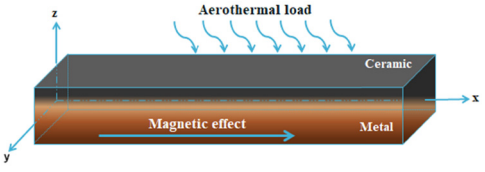

Figure 1: Geometry of the problem.

$$u_x(x, z, \tilde{t}) = -z\frac{\partial w(x, \tilde{t})}{\partial x}, \tag{2.4}$$

$$w_z(x, z, \tilde{t}) = w(x, \tilde{t}). \tag{2.5}$$

Here, u_x be the longitudinal displacement and w_z be the bending components of transverse displacement. The corresponding linear strain–displacement relationship is used, consistent with small deformation assumptions, to describe the mechanical behavior of the FG nanobeam. Thereby [30].

$$\varepsilon_{ij} = \frac{1}{2}\left[\frac{\partial u_i}{\partial j} + \frac{\partial u_j}{\partial i} + \frac{\partial u_k}{\partial i} + \frac{\partial u_k}{\partial j}\right]. \tag{2.6}$$

meanwhile, (i, j, k) are the elements of $[x, y, z]$ while utilizing the equations,

$$\varepsilon_{xx} = -z\frac{\partial^2 w(x, t)}{\partial x^2}. \tag{2.7}$$

Let U be the strain energy and it can be defined as [22],

$$U = \frac{1}{2}\int_0^L\int_A \sigma_{xx}\varepsilon_{xx}\mathrm{d}A\mathrm{d}x, \tag{2.8}$$

where σ_{xx} is the normal stress, A represents the area of cross-section of the beam, and L be the length.

By substituting Eq. (2.7) into Eq. (2.8), the maximum strain energy can be expressed as,

$$U_{\max} = -\frac{1}{2}\int_0^L M\frac{\partial^2 w}{\partial x^2}\mathrm{d}x. \tag{2.9}$$

Consequently, the moment stress equation for the Euler beam can be expressed as,

$$M = \int_A z\sigma_{xx}\mathrm{d}A. \tag{2.10}$$

The maximum kinetic energy can be,

$$T_{\max} = \frac{1}{2}\int_0^L \rho A\varpi^2 w^2\mathrm{d}x, \tag{2.11}$$

where ϖ be the circular frequency.

$$\frac{\partial^2 M}{\partial x^2} = -\rho A\varpi^2 w. \tag{2.12}$$

The constitutive relation with the presence of thermal load is

$$\sigma_{xx} - Q_{11}(\varepsilon_{xx} - \alpha_x\Delta T) = 0. \tag{2.13}$$

$\Delta T = T - T_0$ represents the temperature rise from an initial temperature T_0 to temperature T. Additionally, through axial direction Q_{11} and α_x represents the elastic stiffness coefficient and the thermal expansion coefficient. It can be defined as, $Q_{11} = \frac{E}{1-\nu^2}$.

For FGM nanobeams σ_x, the normal stress can be described as,

$$\sigma_{xx} - (e_0a)^2\frac{\partial^2\sigma_{xx}}{\partial x^2} = \frac{E}{1-\nu^2}\frac{\partial^2 w}{\partial x^2}, \tag{2.14}$$

where $(e_0a)^2$ is the nonlocal parameter, e_0 is a material constant, and a is an internal characteristic length. In this study, it is postulated that the nonlocal parameter undergoes alteration concurrent with the modifications in other material attributes within the FGM. The influence of nonlocal parameters varies along the thickness dimension of FG nanobeam. The connection between nonlocal stress and strain is not solely governed by changes in Young's modulus and Poisson's ratio; it also hinges on variations in the nonlocal parameter. As the FG nanobeam is exposed to an aerodynamic force ΔP perpendicular to its surface (in the z direction) due to supersonic airflow, the unsteady aerodynamic load for high Mach numbers can be described using the first-order Piston theory [30].

$$\Delta P = -\varsigma\frac{\partial w}{\partial x} - \xi\frac{\partial w}{\partial t}, \tag{2.15}$$

where,

$$\varsigma = \frac{\rho_\infty u_\infty^2}{\sqrt{M_\infty^2 - 1}}, \tag{2.16}$$

$$\xi = \frac{\rho_\infty u_\infty (M_\infty^2 - 2)}{(\sqrt{M_\infty^2 - 1})^3}. \tag{2.17}$$

Given, ρ_∞ is density, u_∞ is the velocity, and M_∞ is Mach number of the free stream air, accordingly.

Now multiplying Eq. (2.14) by $z\mathrm{d}A$ and integrating over A gives the equation of nonlocal moment is obtained here. Here, A is the beam's cross-section. Moreover, σ_{xx} is the axial stress in the x direction.

$$\begin{aligned}&\int_A \sigma_{xx}z\mathrm{d}A - \int_A (e_0a)^2\frac{\partial^2\sigma_{xx}}{\partial x^2}z\mathrm{d}A\\ &= \int_A \frac{E}{1-\nu^2}\frac{\partial^2 w}{\partial x^2}z\mathrm{d}A,\end{aligned} \tag{2.18}$$

$$M - (e_0a)^2\frac{\partial^2 M}{\partial x^2} = \frac{E}{1-\nu^2}\frac{\partial^2 w}{\partial x^2}, \tag{2.19}$$

$$M = \frac{E}{1-\nu^2}\frac{\partial^2 w}{\partial x^2} - (e_0a)^2\rho A\varpi^2 w. \tag{2.20}$$

Now by incorporating the external forces into the above equation,

$$M = \frac{E}{1-\nu^2}\frac{\partial^2 w}{\partial x^2} - (e_0 a)^2 \rho A \varpi^2 w + f_B + \Delta P, \quad (2.21)$$

where $f_B = \eta A \Omega_x^2 \frac{\partial^2 w}{\partial x^2}$, f_B is the magnetic field; η is the field permeability; Ω_x stands for magnetic potential.

3 Solution procedures

In this study, the vibration equation of an Euler nanobeam is addressed using BPs. These polynomials possess key properties that are useful for solving nonhomogeneous nonlinear integro-differential equations.

$$B_{n,i}^R(x) = nC_i\, x^i (1-x)^{n-i}, \quad (3.1)$$

whereas $nC_i = n!/(n-1)!i!$. And generally, there are n degrees of BPs. Some particular instances include:

$$\begin{aligned} B_{1,0}^R(x) &= 1 - x, \\ B_{1,1}^R(x) &= x. \end{aligned} \quad (3.2)$$

$$\begin{aligned} B_{2,0}^R(x) &= (1-x)^2, \\ B_{2,1}^R(x) &= 2x(1-x), \\ B_{2,2}^R(x) &= x^2. \end{aligned} \quad (3.3)$$

$$\begin{aligned} B_{3,0}^R(x) &= (1-x)^3, \\ B_{3,1}^R(x) &= 3x(1-x)^2, \\ B_{3,2}^R(x) &= 3x^2(1-x), \\ B_{3,3}^R(x) &= x^3. \end{aligned} \quad (3.4)$$

3.1 Analytical solution

In this section, the Bernstein polynomials (BP's) from the earlier part are used for solving Eq. (2.21) and can be expressed in terms of:

$$W(X) = \sum_{i=0}^{n} c_i \phi_i. \quad (3.1.1)$$

For the simplification in the mathematical modeling, the following nondimensional terms are updated:

For nanobeam length,

$$X = \frac{x}{L}. \quad (3.1.2)$$

For transverse displacement,

$$W = \frac{w}{L}, \quad (3.1.3)$$

where c_i are the unknown constants and n is the approximation order. The shape function of the beam is considered as,

$$\phi_i(X) = \pi_b B_{i,n}^R(X). \quad (3.1.4)$$

In which, the BPs $B_{i,n}(X)$ are considered as

$$B_{i,n}^R(X) = nC_i\ X^i (1-X)^{n-i}, \quad (3.1.5)$$

whereas, the generalized boundary equation of the beam π_b in dimensionless form is given as

$$\pi_b = X^r (1-X)^s, \quad (3.1.6)$$

where r and s are assuming the values among 0, 1, and 2, accordingly free, simply supported, and clamped, respectively.

The material properties considered in this analysis include the effective mass density ρ and effective nonlocal parameter $\mu(z)$. While the nonlocal parameter shows variations across different materials, a variable nonlocal parameter implies that nonlocal effects can vary spatially or with respect to specific parameters within the structure. This parameter adapts to the model, influenced by factors like material properties, dimensions, or environmental conditions. The parameter denoted as $\zeta = \mu_c/\mu_m$ represents the proportion between the ceramic and metal phases. In cases where the nonlocal parameter is constant, ζ equals one ($\zeta = 1$) [31].

In the Rayleigh–Ritz method, by minimizing the total energy of the system, which consists of both kinetic and strain energy,

$$U_{\max} - T_{\max} = 0. \quad (3.1.7)$$

Substituting the Eq. (3.1.1) into the Eq. (3.1.7) and differentiating by parts with the help of unknown coefficients c_i yields the extended eigenvalue problem as

$$[K]\{Y\} = \lambda^2 [M]\{Y\}. \quad (3.1.8)$$

From the above definition, $[K]$ represents stiffness and $[M]$ is for mass matrices. The elements of these matrices are:

$$K = \begin{bmatrix} \int_0^1 \phi_0'' \phi_0'' \mathrm{d}X & \int_0^1 \phi_1'' \phi_0'' \mathrm{d}X & \cdots & \int_0^1 \phi_n'' \phi_0'' \mathrm{d}X \\ \int_0^1 \phi_0'' \phi_1'' \mathrm{d}X & \int_0^1 \phi_1'' \phi_1'' \mathrm{d}X & \cdots & \int_0^1 \phi_n'' \phi_1'' \mathrm{d}X \\ \vdots & \vdots & \vdots & \vdots \\ \int_0^1 \phi_0'' \phi_n'' \mathrm{d}X & \int_0^1 \phi_1'' \phi_n'' \mathrm{d}X & \cdots & \int_0^1 \phi_n'' \phi_n'' \mathrm{d}X \end{bmatrix}, \quad (3.1.9)$$

$$M = \begin{bmatrix} \int_0^1 \phi_0\phi_0 - (\alpha^2+\xi+\varsigma)\phi_0\phi_0'' - \eta\Omega_x^2\phi_0''\phi_0''\mathrm{d}X & \int_0^1 \phi_1\phi_0 - (\alpha^2+\xi+\varsigma)\phi_1\phi_0'' - \eta\Omega_x^2\phi_1''\phi_0''\mathrm{d}X & \cdots & \int_0^1 \phi_n\phi_0 - (\alpha^2+\xi+\varsigma)\phi_n\phi_0'' - \eta\Omega_x^2\phi_n''\phi_0''\mathrm{d}X \\ \int_0^1 \phi_0\phi_1 - (\alpha^2+\xi+\varsigma)\phi_0\phi_1'' - \eta\Omega_x^2\phi_0''\phi_1''\mathrm{d}X & \int_0^1 \phi_1\phi_1 - (\alpha^2+\xi+\varsigma)\phi_1\phi_1'' - \eta\Omega_x^2\phi_1''\phi_1''\mathrm{d}X & \cdots & \int_0^1 \phi_n\phi_1 - (\alpha^2+\xi+\varsigma)\phi_n\phi_1'' - \eta\Omega_x^2\phi_n''\phi_1''\mathrm{d}X \\ \vdots & \vdots & \vdots & \vdots \\ \int_0^1 \phi_0\phi_n - (\alpha^2+\xi+\varsigma)\phi_0\phi_n'' - \eta\Omega_x^2\phi_0''\phi_n''\mathrm{d}X & \int_0^1 \phi_1\phi_n - (\alpha^2+\xi+\varsigma)\phi_1\phi_n'' - \eta\Omega_x^2\phi_1''\phi_n''\mathrm{d}X & \cdots & \int_0^1 \phi_n\phi_n - (\alpha^2+\xi+\varsigma)\phi_n\phi_n'' - \eta\Omega_x^2\phi_n''\phi_n''\mathrm{d}X \end{bmatrix}, \quad (3.1.10)$$

where $\lambda^2 = \frac{(1-\nu)^2\rho A\varpi^2L^4}{E}$ represents frequency parameter, $\{Y\} = [c_0, c_1, \ldots c_n]^T$ are the scalar coefficients of the mass matrix, and $\phi_i'' = \frac{\mathrm{d}^2}{\mathrm{d}X^2}(B_{i,n}^R(X) \cdot \pi_b(X))$ denotes the shape function.

The displacement function assumed in Eq. (3.1.1) converges with the BP given in Eq. (3.1.5). This is demonstrated using the convergence theorem.

3.2 Equations of OBPs

The relation of displacement component is designed as,

$$W(X) = \sum_{i=0}^{n} c_i\hat{\phi}_i, \quad (3.2.1)$$

where $\hat{\phi}_i$'s are orthonormal polynomials, which may be obtained using any orthogonalisation process such as three-term recurrence relation or Gram–Schmidt process. Gram–Schmidt process is used here to find orthonormal polynomials,

$$\theta_i = \pi_b B_{i,n}^R(X), \quad (3.2.2)$$

where $B_{i,n}^R(X)$, π_b are defined in Eqs. (3.1.5) and (3.1.6), respectively.

$$\hat{\phi}_0 = \theta_0, \quad (3.2.3)$$

$$\hat{\phi}_i = \theta_i - \sum_{j=0}^{i-1} \lambda_{ij}\hat{\phi}_j. \quad (3.2.4)$$

In this context, $\lambda_{ij} = \frac{\langle\theta_i,\theta_j\rangle}{\langle\hat{\phi}_i,\hat{\phi}_j\rangle}$.

The inner product <,> in λ_{ij} is taken as $\langle\hat{\phi}_i,\hat{\phi}_j\rangle = \int_0^1\hat{\phi}_i(X)\hat{\phi}_j(X)\mathrm{d}X$, and the norm of $\hat{\phi}_i$ is defined in the following relation,

$$\|\hat{\phi}_i\| = \langle\hat{\phi}_i,\hat{\phi}_i\rangle^{1/2} = \left[\int_0^1\hat{\phi}_i(X)\hat{\phi}_i(X)\mathrm{d}X\right]^{1/2}. \quad (3.2.5)$$

3.3 Convergence theorem

Let us consider the Eq. (4.1),

$$W(X) = \sum_{i=0}^{n} c_i\phi_i = c_0\phi_0 + c_1\phi_1 + \ldots. + c_n\phi_n. \quad (3.3.1)$$

The BPs are known to form a partition of unity,

$$\sum_{i=0}^{n} B_{i,n}^R(X) = 1, \quad X \in [0,1]. \quad (3.3.2)$$

Now, using Eq. (3.1.4) in the Eq. (3.3.1),

$$\begin{aligned} W(X) &= \pi_b\sum_{i=0}^{n} c_iB_{i,n}^R \\ &= \pi_b[c_0B_{0,n}^R + c_1B_{1,n}^R + \ldots + c_nB_{n,n}^R]. \end{aligned} \quad (3.3.3)$$

Here, assume, $c_k = \max\{c_0, c_1, \ldots c_n\}$, then it can be mentioned as,

$$W(X) \le \pi_b c_k[B_{0,n}^R + B_{1,n}^R + \ldots + B_{n,n}^R]. \quad (3.3.4)$$

Using Eq. (3.3.2),

$$W(X) \le \pi_b c_k. \quad (3.3.5)$$

The RHS of Eq. (3.3.5) converges; hence, $W(X)$ also converges.

4 Results and discussion

This section illustrates the magneto-aerothermal vibration of FG Nanobeam with numerical examples. Table 1 presents the material properties composed of $BaTiO_3$,

Table 1: Material properties of $BaTiO_3$ and $CoFe_2O_4$

Material		Properties		
$BaTiO_3$	E [Pa]	166	e_{33} (N/m^2 K)	(7.124 × 10^{-9})
	ρ [kg/m^3]	5,800		
	ν [-]	1.1945	e_{15} (c/m^2)	14.1
$CoFe_2O_4$	E [Pa]	286	e_{31} (c/m^2)	−(4.1)
	ρ [kg/m^3]	5,300		
	ν [-]	1.167	e_{11} (c/Vm)	(5.841 × 10^{-9})

$CoFe_2O_4$ respectively, and Table 2 presents the slenderness ratio of FG nanobeam with poisson ratio and without Poisson's ratio. Based on the results and literature by Alimoradzadeh *et al.* [30], it shows high accuracy to the proposed model.

4.1 Effect of variable nonlocal on axial vibrations of FG nanobeam

In Figure 2, the variable nonlocality in the ceramic phase increases with greater displacement over time. When the μ_c value hits zero, the displacement starts decreasing at time T = 1, then shows an increasing trend, reaching around 2.5. When μ_c = 0.1, the displacement graph similarly increases and decreases around 2.2. As the μ_c value increases to 0.2, the oscillations are higher, and the displacement settles later. Thus, with increasing μ_c value, the graph becomes more amplified and takes longer to stabilize. Compared to ceramics, in Figure 3, the metal experiences greater vibrations. When μ_m = 0, the vibrations start at a higher level and take a long time to settle. As the μ_m increases to 0.1, the time between oscillations decreases compared to zero nonlocal value. With further increases in the nonlocal μ_m value, the amplitude of the oscillations increases before eventually decaying. The initial decay in displacement followed by periodic increases and decreases represents a typical damped vibration response, indicating periodic energy exchanges within the material.

Table 2: Comparison table for a slenderness ratio of a FG nanobeam

L/h	Alimoradzadeh *et al.* [30]		Present study	
	$\nu = 0$	$\nu \neq 0$	$\nu = 0$	$\nu \neq 0$
5.0	0.4676	0.4947	0.4676	0.4947
10.0	0.2338	0.2474	0.2338	0.2473
15.0	0.1559	0.1649	0.1558	0.1649
20.0	0.1691	0.1237	0.1690	0.1236
30.0	0.0779	0.0825	0.0779	0.0825
50.0	0.0468	0.0495	0.0467	0.0495

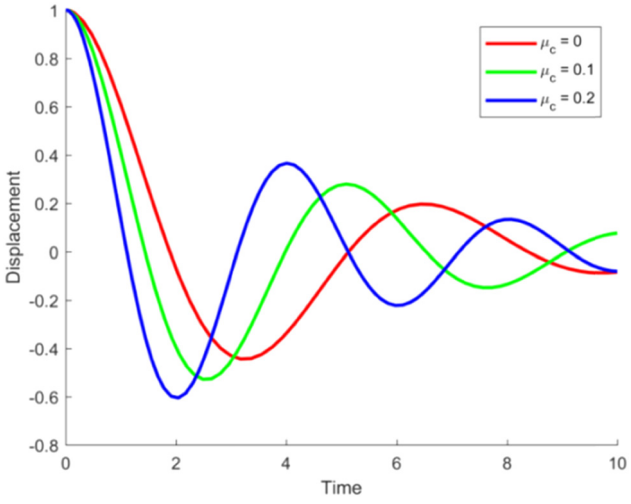

Figure 2: Effect of variable nonlocal (ceramic phase) on axial vibrations: Displacement *vs* time.

Higher nonlocal values increase the amplitude and response time of the material to external forces, leading to larger vibrations. In applications like sensors and actuators, where precise control of vibrations is crucial, adjusting the nonlocal parameter can help achieve the desired dynamic responses.

4.2 Impact of Mach number on axial vibrations in FG nanobeam with different ceramic and metal phases

The effects of variable nonlocal vibration on displacement over time with varying M_∞ on axial vibration are illustrated

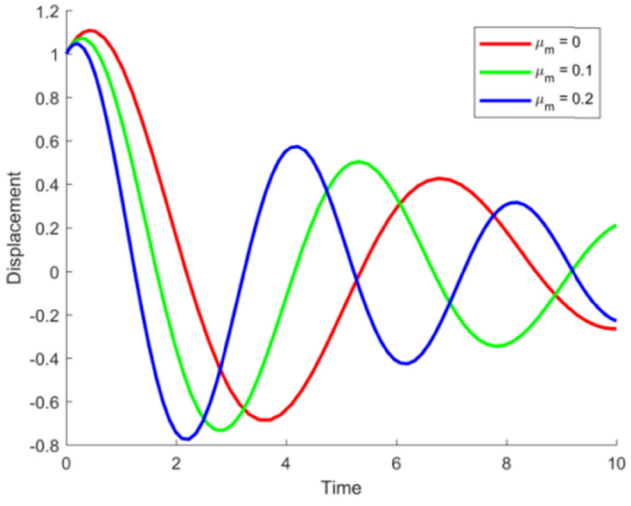

Figure 3: Effect of variable nonlocal (metal phase) on axial vibrations: Displacement *vs* time.

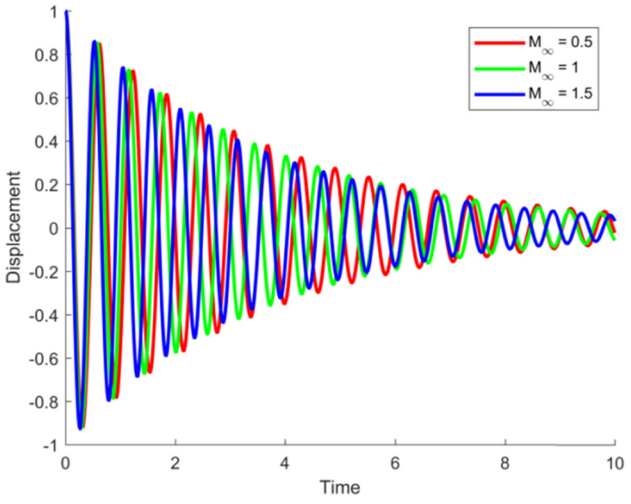

Figure 4: Effect of Mach number on axial vibration (ceramic phase) of FG nanobeam: Displacement *vs* time.

in Figures 4 and 5. In Figure 4, as the M_∞ increase (0.5, 1, 1.5), the displacement oscillates between −1 and 1 for the ceramic phase of the FG nanobeam. Higher Mach numbers lead to high-frequency oscillations with larger amplitudes. Similarly, in Figure 5, for M_∞ = 1.5, the oscillations become more pronounced over a given period. In the metal phase, displacement also shows high-frequency oscillations but with less risk of sudden failure compared to the ceramic phase. The damping is more gradual, allowing for sustained vibrations over a longer period. The metal phase exhibits a slower decay in displacement due to its higher capacity for energy absorption and dissipation.

4.3 Effect of frequency over free stream velocity with varying ceramic and metal phase

At high frequencies, the ceramic phase exhibits significant stiffness, causing the nanobeam to respond with higher resistance to deformation. In Figure 6, the frequency over free stream velocity increases with increasing μ_c value. When μ_c = 0.5, the frequency increases to 1×10^{-3}, and the free stream velocity shows a gradual upward trend. As the μ_c values increase to 1 and 1.5, the frequency decreases gradually around 0.5 to 0.8, with an upward trend in free stream velocity. Similarly, in Figure 7, for μ_m = 0.5, the frequency increase is more pronounced than in the ceramic phase. When the μ_m values reach 1 and 1.5, the frequency decreases with an increasing trend in free stream velocity. Hence, these cases widely happen in aircraft wing design for a precise control of vibrations, enhancing structural integrity and aerodynamic efficiency.

4.4 Effect of position along the length of the nanobeam and variable nonlocal over thermal stress

From Figure 8, the thermal stress along the length of the nanobeam for the ceramic phase starts from a low value at the beginning (x = 0) and increases monotonically towards the end of the beam, reaching its maximum at the free end (x = 1). This trend indicates that the highest thermal stress occurs at the tip of the nanobeam under the given conditions. Higher nonlocal parameters typically distribute stress more

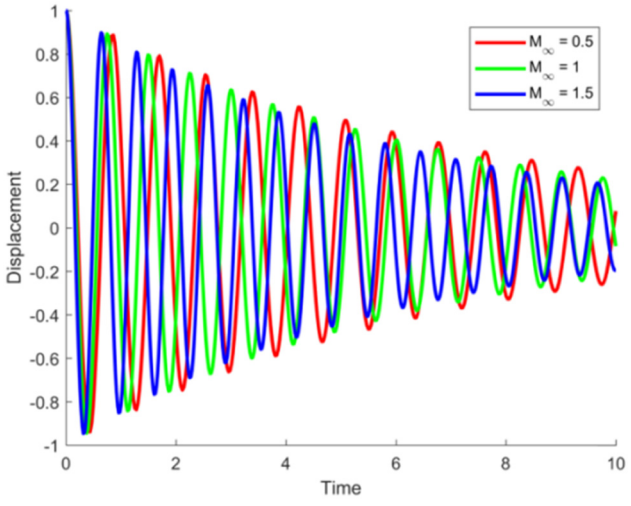

Figure 5: Effect of Mach number on axial vibration (metal phase) of the FG nanobeam: Displacement *vs* time.

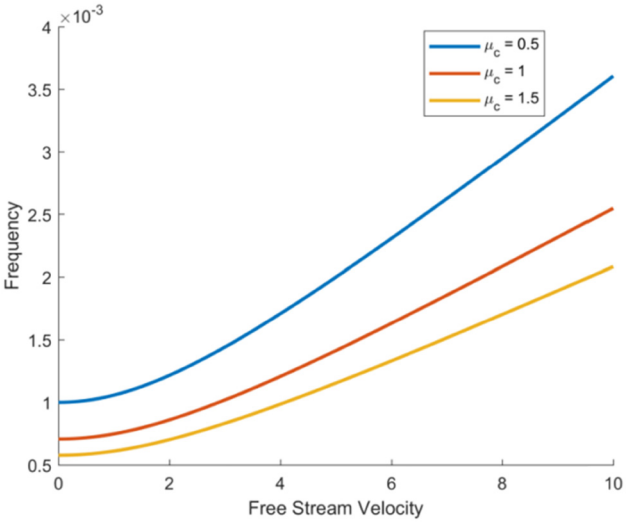

Figure 6: Effect of frequency over free stream velocity for variable nonlocal (ceramic phase).

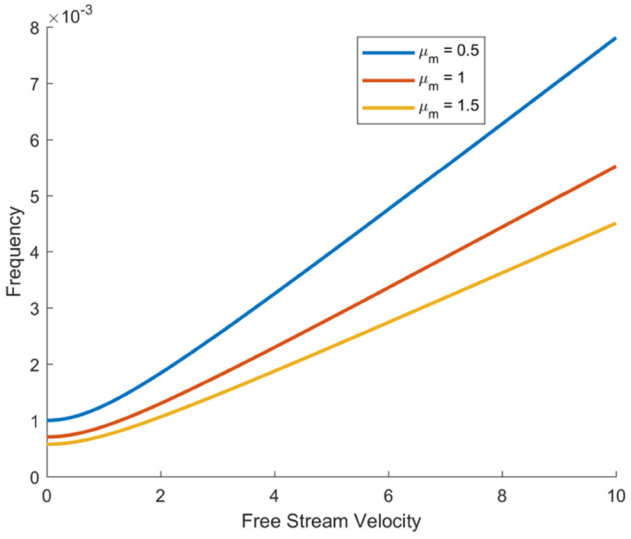

Figure 7: Effect of frequency over free stream velocity for variable nonlocal (metal phase).

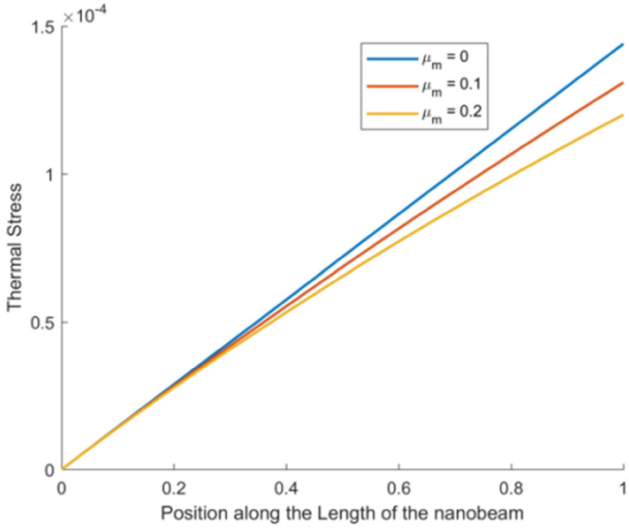

Figure 9: Effect of thermal stress over position along the length of the nanobeam with varying variable nonlocal (metal phase).

evenly, potentially reducing peak stress levels. Similarly, from Figure 9, the thermal stress along the length of the nanobeam for the metal phase increases continuously and reaches its maximum value at the free end (x = 1). Although the overall behavior is similar to the ceramic phase, the magnitude of the peak stress differs due to the higher thermal conductivity and different thermal expansion properties of metals. Metals, having higher thermal conductivity than ceramics, tend to exhibit a more uniform temperature distribution, which can reduce thermal gradients and potentially lower thermal stresses. Higher nonlocal parameters in the metal phase also contribute to a more even stress distribution and a slight reduction in peak stresses.

4.5 Effect of velocity over magnetic potential for ceramic and metal phases

In Figure 10, the contour lines indicate specific values of magnetic potential across varying velocities. The intensity at 0.02 to 0.04 suggests that the magnetic potential remains relatively stable or reaches a critical point at this value. Similarly, from 0.04 to 0.06, the magnetic potential intensifies to 0.004–0.006. In Figure 11, the metal phase exhibits a more intense reaction, with magnetic potential reaching above 0.005 compared to the ceramic phase. This indicates a significant point where the nanobeam may exhibit

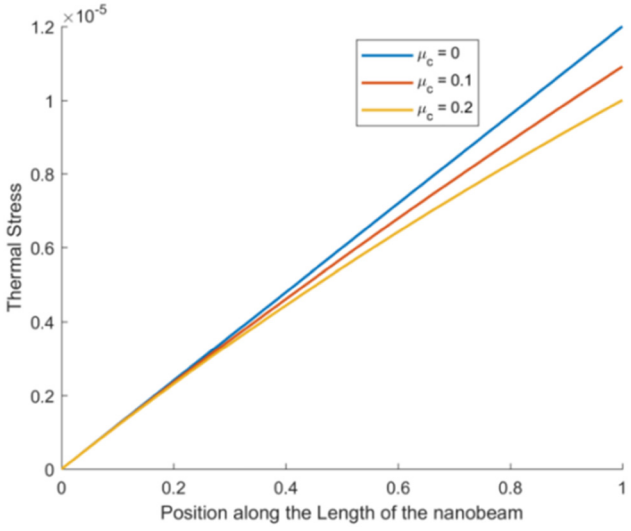

Figure 8: Effect of thermal stress over position along the length of the nanobeam with varying variable nonlocal (ceramic phase).

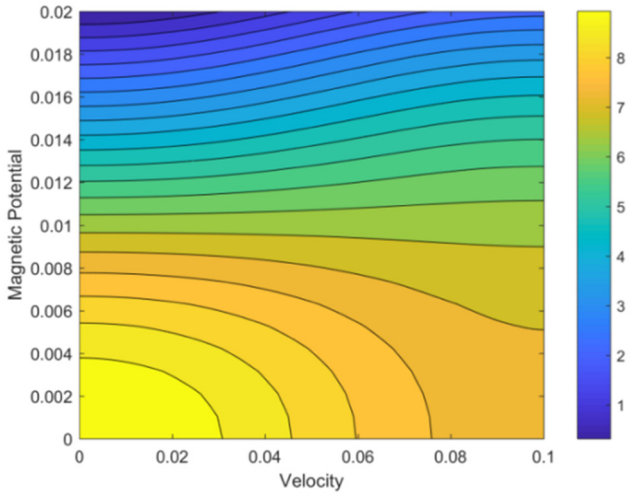

Figure 10: A contour plot for magnetic potential over velocity for the ceramic phase of FG nanobeam.

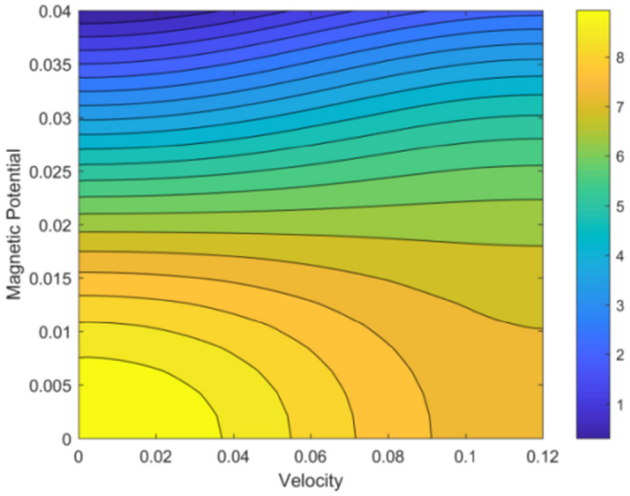

Figure 11: A contour plot for magnetic potential over velocity for the metal phase of FG nanobeam.

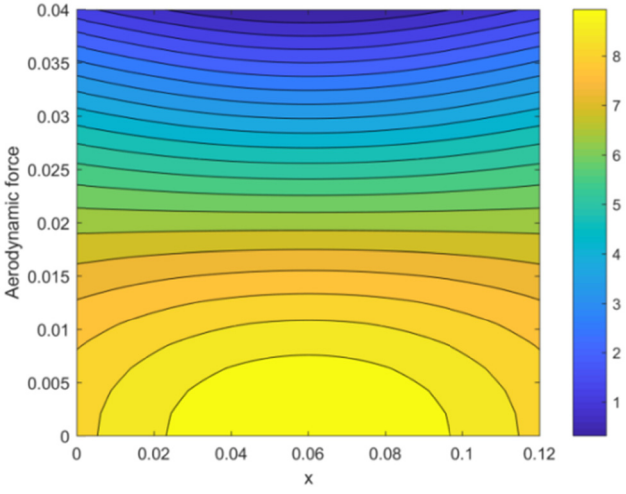

Figure 13: A contour plot for aerodynamic force over x for the metal phase of FG nanobeam.

enhanced magnetic response or stability under specific velocity conditions for both ceramic and metal phases. The intensification and coloring of contours at specific magnetic potential levels in both figures highlight critical points and gradients, offering a nuanced understanding of magnetic behavior under different operational conditions.

4.6 Effect of aerodynamic force over length for ceramic and metal phases

The contour plot in Figures 12 and 13 illustrates variations in aerodynamic force across the x in the FG nanobeam for both ceramic and metal phases of the nanobeam. Intensified contours suggest regions of higher aerodynamic force, potentially influenced by the structural stiffness and surface characteristics of the ceramic material. In contrast, metal contours display a broader but less intense distribution, indicating the material's damping capacity and flexibility under aerodynamic loads.

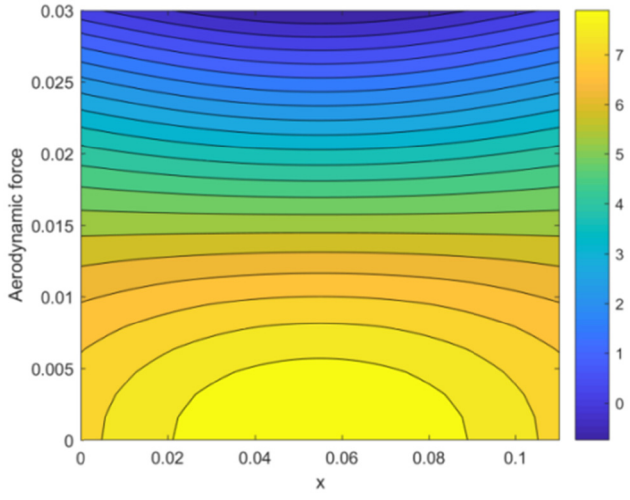

Figure 12: A contour plot for aerodynamic force over x for the ceramic phase of FG nanobeam.

5 Conclusions

The study presented above investigates the interplay between the nonlocal parameter and material variations in FG nanobeams under unsteady aerodynamic thermal loads, defined by the first-order piston theory. The governing equations for FG Euler nanobeams were formulated by using Eringen's nonlocal elasticity theory and numerically tested through the Bernstein-based Rayleigh-Ritz method. The results demonstrate a strong correlation with previously published data, affirming the accuracy and reliability of the current model. Furthermore, the study reveals a significant impact of nonlocal ceramic and metal components on the key parameters such as magnetic potential and aerodynamic pressure on the FG nanobeam. These findings contribute to a deeper understanding of the behavior of FG nanobeams, paving the way for enhanced design and optimization in advanced engineering applications. Moreover, graphical solutions are presented to illustrate the dispersion subjected to aero thermal loads and external factors as magnetic fields incorporating the influence of both ceramic and metal properties, thereby offering insights into the

influence of these variables on the nanobeam's vibrational behavior. Key findings are summarized as follows:

- At higher Mach numbers, the nanobeam experiences increased natural frequencies and enhanced aerodynamic damping, resulting in quicker dissipation of vibrational energy and affecting the displacement decay rate.
- As free-stream velocities rise, aerodynamic forces on the FG nanobeam intensify, leading to notable alterations in natural frequencies and damping characteristics.
- The thermal stress along the nanobeam's length peaks at the free end, with both ceramic and metal phases experiencing maximum stress, though the metal phase shows a more uniform distribution due to its higher thermal conductivity.
- Higher velocities amplify aerodynamic forces, intensifying dynamic responses and increasing the risk of resonance and flutter phenomena in both metallic and ceramic phases, thereby impacting structural stability.
- Elevated stresses in the metallic phase predominantly lead to increased bending and torsional effects, whereas in the ceramic phase, localized stress concentrations and vibrational behaviors emerge, influencing the nanobeam's performance and durability.
- The findings can serve as benchmark results for future studies focusing on the dynamic analysis of nanostructures under variable small-scale parameters and aerothermal conditions. Further integration with multi-physics experimental setups and consideration of material degradation over time would enhance the practical applicability of the model for advanced engineering applications.

Funding information: The authors state no funding involved.

Author contributions: RS and PT: data curation, formal analysis, model design, numerical validation. RS and RD: software writing, writing original draft, investigation methodology. RS and LR: conceptualization, methodology, final write-up, mathematical validation, visualization, writing review. RS and FT: editing and numerical analysis. All authors have accepted responsibility for the entire content of this manuscript and consented to its submission to the journal, reviewed all the results and approved the final version of the manuscript.

Conflict of interest: Rossana Dimitri and Francesco Tornabene, who are the co-authors of this article, are current Editorial Board members of Curved and Layered Structures. This fact did not affect the peer-review process. Authors declare no other conflict of interest.

References

[1] Ebrahimi F, Karimiasl M, Singhal A. Magneto-electro-elastic analysis of piezoelectric–flexoelectric nanobeams rested on silica aerogel foundation. Eng Comput. 2021;37:1007–14. doi: 10.1007/s00366-019-00869-z.

[2] Ebrahimi F, Khosravi K, Dabbagh A. Wave dispersion in viscoelastic FG nanobeam via a novel spatial–temporal nonlocal strain gradient framework. Waves Random Complex Media. 2021;31(8):1–23. doi: 10.1080/17455030.2021.1970282.

[3] Ebrahimi F, Barati MR. Vibration analysis of smart piezoelectrically actuated nanobeams subjected to magneto-electrical field in thermal environment. J Vib Control. 2018;24:549–64. doi: 10.1177/1077546316646239.

[4] Nguyen TK, Nguyen TT, Vo TP, Thai HT. Vibration and buckling analysis of functionally graded sandwich beams by a new higher-order shear deformation theory. Compos Part B: Eng. 2015;76:273–85. doi: 10.1016/j.compositesb.2015.02.032.

[5] Alibeigi B, Tadi Beni Y, Mehralian F. On the thermal buckling of magneto-electro-elastic piezoelectric nanobeams. Eur Phys J Plus. 2018;133:1–18. doi: 10.1140/epjp/i2018-11954-7.

[6] Alibeigi M, Farahani SD. Effect of porous medium positioning on heat transfer of micro-channel with jet. Int J Eng. 2020;33(10):2057–64. doi: 10.5829/ije.2020.33.10c.19.

[7] Shariati A, Ebrahimi F, Karimiasl M, Selvamani R, Toghroli A. On bending characteristics of smart magneto-electro-piezoelectric nanobeams system. Adv Nano Res. 2020;9(3):183–91. doi: 10.12989/anr.2020.9.3.183.

[8] Ebrahimi F, Karimiasl M, Selvamani R. Bending analysis of magneto-electro piezoelectric nanobeams system under hygro-thermal loading. Adv Nano Res. 2020;8:203–14. doi: 10.12989/anr.2020.8.3.203.

[9] Li SR, Su HD, Cheng CJ. Free vibration of functionally graded material beams with surface-bonded piezoelectric layers in thermal environment. Appl Math Mech. 2009;30:969–82. doi: 10.1007/s10483-009-0803-7.

[10] Romano G, Barretta R. Stress-driven versus strain-driven nonlocal integral model for elastic nano-beams. Compos Part B: Eng. 2017;114:184–8. doi: 10.1016/j.compositesb.2017.01.008.

[11] Barretta R, Fabbrocino F, Luciano R, Sciarra FM. Closed-form solutions in stress-driven two-phase integral elasticity for bending of functionally graded nano-beams. Phys E: Low-Dimension Syst Nanostruct. 2018;97:13–30. doi: 10.1016/j.physe.2017.09.026.

[12] Kiani Y, Eslami MR. Thermal buckling analysis of functionally graded material beams. Int J Mech Mater Des. 2012;6:229–38. doi: 10.1007/s10999-010-9132-4.

[13] Sun D, Luo SN. Wave propagation of functionally graded material plates in thermal environments. Ultrasonics. 2011;51(8):940–52. doi: 10.1016/j.ultras.2011.05.009.

[14] Thai HT, Choi DH. A refined shear deformation theory for free vibration of functionally graded plates on elastic foundation. Compos Part B: Eng. 2012;43(5):2335–47. doi: 10.1016/j.compositesb.2011.11.062.

[15] Thai HT, Park T, Choi DH. An efficient shear deformation theory for vibration of functionally graded plates. Arch Appl Mech. 2013;83(1):137–49. doi: 10.1007/s00419-012-0642-4.

[16] Reddy JN, El-Borgi S. Eringen's nonlocal theories of beams accounting for moderate rotations. Int J Eng Sci. 2014;82:159–77. doi: 10.1016/j.ijengsci.2014.05.006.

[17] Ebrahimi F, Barati MR. Size-dependent vibration analysis of viscoelastic nanocrystalline silicon nanobeams with porosities based on a higher-order refined beam theory. Compos Struct. 2017;166:256–67. doi: 10.1016/j.compstruct.2017.01.036.
[18] Lim CW, Zhang G, Reddy JN. A higher-order nonlocal elasticity and strain gradient theory and its applications in wave propagation. J Mech Phys Solids. 2015;78:298–313. doi: 10.1016/j.jmps.2015.02.001.
[19] Ebrahimi F, Mokhtari M. Transverse vibration analysis of rotating porous beam with functionally graded microstructure using the differential transform method. J Braz Soc Mech Sci Eng. 2015;37:1435–44. doi: 10.1007/s40430-014-0232-2.
[20] Ebrahimi F, Salari E. Effect of various thermal loadings on buckling and vibrational characteristics of nonlocal temperature-dependent functionally graded nanobeams. Mech Adv Mater Struct. 2016;23:1379–97. doi: 10.1080/15376494.2015.1091524.
[21] Vinh PV, Tounsi A. The role of spatial vibration of the nonlocal parameter on the free vibration of functionally graded sandwich nanoplates. Eng Comput. 2022;38(Suppl 5):4301–19. doi: 10.1007/s00366-021-01475-8.
[22] Karmakar S, Chakraverty S. Boundary characteristic Bernstein polynomials based solution for free vibration of Euler nanobeams. J Compos Sci. 2019;3(4):99. doi: 10.3390/jcs3040099.
[23] Li L, Hu Y. Nonlinear and free vibration analysis of nonlocal strain gradient beams made of functionally graded material. Int J Eng Sci. 2016;102:77–92. doi: 10.1016/j.ijengsci.2016.07.011.
[24] Ke LL, Wang YS. Free vibration of size-dependent magneto-electro-elastic nanobeams based on the nonlocal theory. Phys E: Low-Dimension Syst Nanostruct. 2014;63:52–61. doi: 10.1016/j.physe.2014.05.002.
[25] Mohamed SA, Mohamed NA, Abo-Bakr RM, Eltaher MA. Multi-objective optimization of snap-through instability of helicoidal composite imperfect beams using Bernstein polynomials method. Appl Math Model. 2023;120:301–29. doi: 10.1016/j.apm.2023.03.034.
[26] Selvamani R, Prabhakaran T, Rubine L, Jayan M, Wang L. Vibration of nonhomogeneous porous Euler nanobeams using Bernstein polynomials for boundary characteristics. Songklanakarin J Sci Technol. 2024;46(2):6. doi: 10.14456/sjst.2024.6.
[27] Selvamani R, Prabhakaran T, Ebrahimi F. Damping characteristics of nonlocal strain gradient waves in thermoviscoelastic graphene sheets subjected to nonlinear substrate effects. Phys Mesomechanics. 2024;27(4):461–71. doi: 10.1134/S1029959924040106.
[28] Prabhakaran T, Selvamani R, Mahaveersreejayan M, Wang L. Investigation of the effect of viscosity and density on the wave propagation of a nonlocal porous beam submerged in fluid using Bernstein polynomials. Eng Trans. 2024;72(3):365–85. doi: 10.24423/EngTrans.3277.2024.
[29] Selvamani R, Thangamuni P, Yaylacı M, Özdemir ME, Yaylacı EU. Nonlinear vibration and parametric excitation of magneto-thermo elastic embedded nanobeam using homotopy perturbation technique. ZAMM-J Appl Math Mech/Z Angew Math Mech. 2024;104:e202400525. doi: 10.1002/zamm.202400525.
[30] Alimoradzadeh M, Tornabene F, Dimitri R. Nonlinear axial-lateral coupled vibration of functionally graded-fiber reinforced composite laminated (FG-FRCL) beams subjected to aero-thermal loads. Int J Non-Linear Mech. 2024;1(159):104612. doi: 10.1016/j.ijnonlinmec.2023.104612.
[31] Tao C, Fu YM, Dai HL. Nonlinear dynamic analysis of fiber metal laminated beams subjected to moving loads in thermal environment. Compos Struct. 2016;140:410–6. doi: 10.1016/j.compstruct.2015.12.011.